Emergent Materials
https://doi.org/10.1007/s42247-022-00418-3

ORIGINAL ARTICLE

A drug-eluting nanofibrous hyaluronic acid-keratin mat for diabetic wound dressing

Sena Su[1,2] · Tuba Bedir[1,3] · Cevriye Kalkandelen[1,4] · Hilal Turkoglu Sasmazel[5] · Ahmet Ozan Basar[5] · Jing Chen[6] · Nazmi Ekren[1,7] · Oguzhan Gunduz[1,3]

Received: 4 August 2022 / Accepted: 20 September 2022

Abstract
Diabetes mellitus is a chronic metabolic disease associated with long-term multisystem complications, among which are non-healing diabetic foot ulcers (DFUs). Electrospinning is a sophisticated technique for the preparation of polymeric nanofibers impregnated with drugs for wound healing, burns, and diabetic ulcers. This study describes the fabrication and characterization of a novel drug-eluting dressing made of core–shell structured hyaluronic acid (HA)–keratin (KR)-polyethylene oxide (PEO) and polycaprolactone (PCL) nanofibers to treat diabetic wounds. The core–shell nanofibers produced by the emulsion electrospinning technique provide loading of metformin hydrochloride (MH), HA, and KR in the core of nanofibers, which in return improves the sustained long term release of the drug and prolongs the bioactivity. Morphological and chemical properties of the fibers were examined by SEM, FTIR, and XRD studies. It was observed that the fibers which contain HA and KR showed thin fiber structure, greater swelling capacity, fast degradation and increased cumulative drug release amount than neat emulsion fibers due to the hydrophilic nature of HA and KR. MH showed a sustained release from all fiber samples over 20 days and followed the first-order and Higuchi model kinetics and Fickian diffusion mechanism according to kinetic analysis results. In vitro cell culture studies showed that the developed mats exhibited enhanced biocompatibility performance with HA and KR incorporation. The results show that HA and KR-based emulsion electrospun fiber mats are potentially useful new nanofiber-based biomaterials in their use as drug carriers to treat diabetic wounds.

Keywords Drug release · Metformin hydrochloride · Emulsion electrospinning · Natural polymers · Wound healing

1 Introduction

Diabetes mellitus is a metabolic disease characterized by elevated serum glucose levels caused by changes in insulin secretion, insulin action, or both [1]. The peripheral vascular dysfunction, diabetic peripheral neuropathy, and a weakened healing cascade that develops in diabetic individuals lead to the progression of diabetic foot ulcer (DFU) [2]. Wound healing is a complex process that includes hemostasis/coagulation, inflammation, proliferation (granulation tissue

✉ Oguzhan Gunduz
ucemogu@ucl.ac.uk

1 Center for Nanotechnology and Biomaterials Application and Research, Marmara University, 34722 Istanbul, Turkey

2 Department of Bioengineering, Faculty of Chemical and Metallurgical Engineering, Yildiz Technical University, 34210 Istanbul, Turkey

3 Department of Metallurgical and Materials Engineering, Faculty of Technology, Marmara University, 34722 Istanbul, Turkey

4 Biomedical Devices Technology, Vocational School Technical Science, Istanbul University-Cerrahpasa, 34500 Istanbul, Turkey

5 Metallurgical and Materials Engineering Department, Faculty of Engineering, Atilim University, Incek, 06830 Ankara, Turkey

6 Zhejiang Engineering Research Center for Biomedical Materials, Cixi Institute of Biomedical Engineering, Ningbo Institute of Materials Technology and Engineering, Chinese Academy of Sciences, Ningbo 315300, China

7 Department of Electrical and Electronics Engineering, Faculty of Technology, Marmara University, 34722 Istanbul, Turkey

Published online: 04 October 2022

formation), re-epithelialization, and remodelling [3, 4]. In diabetic patients, the healing process does not fit this pattern but instead is concluded with chronic non-healing wounds that pause in one or more of the aforementioned healing phases [5]. To improve the healing process, wound care comprises standards such as removing dead tissue, cleaning the wound area, and dressing [6, 7]. Although an ideal dressing provides a suitable environment for rapid wound healing [8], diabetic wounds are more necrotic, more exudative, and deeper than normal wounds, requiring sophisticated wound care measures [9]. In the wound healing process, local delivery of drugs is favored due to its advantages such as reducing the side effects on a tissue, increasing the efficiency of drug therapy, alleviating the replacement of dressing, and decreasing bacterial resistance [10]. Nowadays, nanofiber dressings are especially prominent as a means of delivering therapeutic agents to wound areas [11]. In this context, it has become highly substantial to develop novel bioactive nanofibrous mat/wound dressings compared to conventional wound care products for rapid wound healing applications.

Recently, electrospinning (ES) has attracted significant attention for producing scaffolds in wound healing applications. ES is a versatile, straightforward, and robust technique for producing fibrous scaffolds comprise of various polymers with controlled surface morphology and with nano- to micrometer range diameters [12]. Electrospun nanofibers mimic the natural extracellular matrix (ECM) that ensures cell adhesion, migration and proliferation [13, 14], as well as their high surface-area-to-volume ratio with an interconnected porous network, allows oxygen permeation, absorption of wound exudates, protection of the wound area from dehydration, prevention of bacterial colonization, and exchanging fluids [15, 16]. Moreover, ES enables the incorporation of bioactive and/or therapeutic agents (e.g., anti-inflammatory drugs, growth factors, antimicrobial, and anaesthetics), thereby improving the biological behaviour of wound dressings.[14, 15, 16, 17-18]

The versatile nature of the core/shell structured nanofibers provides the desired properties for the drug delivery system and tissue-engineered scaffolds [19]. The core part of a nanofiber can ensure the appropriate environment for the drug, while the shell part can act as a barrier to obstruct the early release of the drug in the core [20, 21]. Coaxial ES and emulsion ES are among the main techniques for fabricating core/shell nanofibers [22, 23]. Emulsion ES uses only a single nozzle to obtain core/shell nanofibers compared to coaxial electrospinning, which uses concentric nozzles [24, 25]. This technique is based on dissolving a hydrophilic drug in water (water phase) and a hydrophobic polymer in a solvent (oil phase). As the oil phase vaporizes rapidly during the spinning process, a big part of the hydrophilic drug is encapsulated within the fibers rather than escaping to the fiber surfaces [26], thereby reducing or preventing undesired drug burst release [7]. In addition, this technique offers lower complexity and higher efficiency and reproducibility compared to coaxial [27].

Natural polymers have been widely used in developing electrospun wound dressings, with their excellent biocompatibility, biodegradability, low antigenicity, and bioactivity that promote cell attachment and proliferation [28, 29]. Hyaluronic acid (HA) is a glycosaminoglycan found in the ECM of connective tissues and has unique viscoelastic and mucoadhesive properties for effective wound dressings [30, 31]. Besides, HA has crucial roles in various biological processes, including wound healing [32]. However, electrospinning of HA is a challenge, even at low concentrations, due to its high viscosity and surface tension [30]. HA can blend with other polymers to change its viscosity, thus eliminating the difficulty in electrospinning [32]. Keratin (KR) is a fibrous structural protein that forms the outer covers of the body, such as wool, feathers, hair, nails, horns, and hooves [33, 34]. It is convenient for wound dressing because it supports the structural durability of tissues and cell differentiation and accelerates wound healing by interacting with the proteolytic wound environment [33–35]. The limitation of keratin-based nanofibers is their brittleness [36]. To overcome this, keratin can blend with other polymers, so its spinnability can be improved [37].

Poor healing and diabetes-related wounds are the most critical complications in the acute phase of skin injuries [38]. Metformin hydrochloride (MH), a biguanide derivative, is one of the first choice antihyperglycemic agents worldwide in the treatment of type 2 diabetes [39, 40]. In addition to reducing blood glucose, MH is an insulin booster and may enhance insulin sensitivity [40, 41]. Lee et al. [42] investigated the effect of MH-eluting PLGA nanofibrous membranes on treating diabetes-related wounds. Notably, the addition of MH highly improved the hydrophilicity and water uptake capacity of PLGA. MH-eluting PLGA membranes resulted in faster wound healing and better re-epithelization in diabetic rats. This demonstrated the potential of MH for the treatment of diabetic wounds.

In this study, we present the preparation and characterization of core/shell structured composite nanofibers containing a blend of polyethylene oxide (PEO), keratin (KR), hyaluronic acid (HA), and metformin hydrochloride (MH) encapsulated with a polycaprolactone (PCL) layer using emulsion electrospinning technique. PCL was chosen as the shell material to act as a protective barrier due to its hydrophobic nature, biocompatibility, non-toxicity, and biodegradability [43]. PEO was used as an aqueous polymeric matrix for improving the encapsulation and controlled release of the drug and bioactive compounds [44]. The morphological and chemical properties of the drug-loaded electrospun nanofibers were characterized by scanning electron microscopy (SEM), Fourier transform infrared spectroscopy (FT-IR),

and X-ray diffraction (XRD). Moreover, in vitro drug release behaviour and kinetics and cytocompatibility of the nanofibers were studied.

2 Materials and methods

2.1 Materials

Polycaprolactone (PCL, $M_w = 80{,}000$ g/mol) and Tween-80 (surfactant) were purchased from Sigma-Aldrich, UK. Polyethylene oxide (PEO, $M_w = 600$ g/mol) and metformin hydrochloride were obtained from Sigma-Aldrich, USA. Dimethylformamide (DMF) and chloroform were purchased from Merck KGaA, Germany.

2.2 Fabrication of drug-loaded nanofiber mats with core/shell structure

Drug-loaded nanofibers were fabricated using the emulsion ES technique. The procedure for the extraction of KR and HA was explained in detail in our previously published study [45]. To prepare emulsion spinning solutions, 8% (w/v) solution of PCL was dissolved in chloroform:dimethylformamide mixture with a ratio of 12:1 (v/v), and 1 wt% emulsifier (Tween-80) was added to the solution to form oil phase. PEO was dissolved in distilled water to prepare a 4% (w/v) solution as the water phase. Then, a certain amount of metformin hydrochloride (MH) (10 mg), 2 wt% KR, and 2 wt% HA were added separately and together (1 wt% KR:1 wt% HA) into the PEO solution (aqueous solution) under constant stirring. The aqueous solution was added to the oil solution dropwise, and the mixture was stirred at 240 rpm for 2 h to obtain uniform emulsions. The emulsion solution was transferred to a 10 mL syringe pump with a right angle-shaped needle diameter of (OD: 1.3 mm, ID: 1.2 mm) attached to it. For ES, the solution flow rate was 0.6 to 0.8 mL/h, the range of applied positive voltage was 21 to 24 kV, and the distance between the needle tip and the grounded collector was 19 cm. All ES processes were carried out under ambient conditions. The details of the core and shell solutions were shown in Table 1. Electrospun fibers with an average thickness of 0.2 ± 0.01 mm were produced. The schematic illustration of the produced core–shell structured nanofibers by emulsion electrospinning was presented in Fig. 1.

Table 1 Components of core/shell solutions for emulsion ES

Samples	Shell	Core
MH	8wt% PCL	4wt% PEO + MH
MH-HA	8wt% PCL	4wt% PEO + 2wt% HA + MH
MH-KR	8wt% PCL	4wt% PEO + 2wt% KR + MH
MH-HA + KR	8wt% PCL	4wt% PEO + 1wt% HA + 1wt% KR + MH

2.3 Scanning electron microscopy

The morphology of electrospun nanofibers was studied by scanning electron microscope (EVA MA 10, ZEISS, San Diego, CA, USA) at an accelerating voltage of 10 kV. First, the nanofiber samples on the aluminium foil were coated with a thin layer of gold by a sputter coater (SC7620, Quorum, Lewes, UK). The fiber diameter and diameter distribution were determined by measuring 100 random fibers from SEM micrographs using imaging analysis software (SmartSEM, Zeiss, San Diego, CA, USA).

2.4 Fourier transform-infrared spectroscopy

The chemical structure of nanofiber composites was performed using a Fourier transform infrared spectroscopy (FTIR, JASCO-4000). Infrared absorbance spectra of the samples were analyzed in the wavelength range of 4000 to 400 cm^{-1} at 4 cm^{-1} resolution.

2.5 X-ray diffraction studies

X-ray diffraction (XRD) was used to examine the effect of the drug on the crystalline structure of polymer nanofibers. The XRD patterns of HA and KR powders, drug, and composite fibers were determined using a diffractometer (Shimadzu-6100, Japan).

2.6 Swelling and degradation studies

The swelling degree and weight loss of the nanofiber mats were investigated in a phosphate buffer solution (PBS) (pH = 7.4) at certain time intervals. For the swelling test,

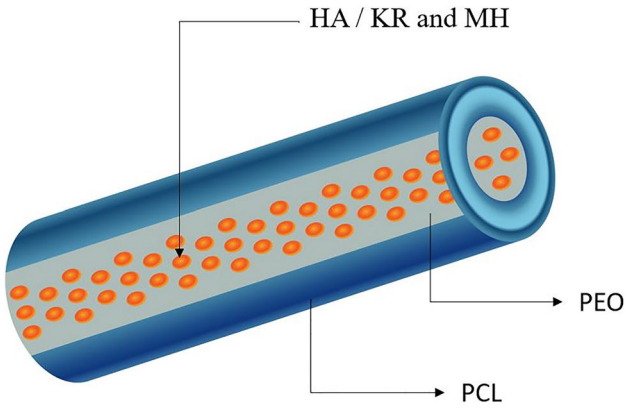

Fig. 1 Schematic illustration of the produced core–shell structured nanofibers

the samples were immersed in PBS medium at 37 °C for 1, 3, 6, 12, and 24 h. The degree of swelling of the samples was calculated using Eq. (1) [46]:

$$\text{Degree of swelling } (\%) = \frac{M - M_d}{M_d} \times 100 \quad (1)$$

where M_d is the weight of the samples before immersion in the PBS medium and M is the weight of the samples after immersion for specific time intervals (t).

The degradation rate (weight loss %) of the samples was determined by drying the samples at ambient conditions until reaching a fixed weight and reweighting at 1, 2, 4, 7, 14, and 21 days. The weight loss of the samples was calculated according to Eq. (2):

$$\text{Weight loss } (\%) = \frac{M_d - M_i}{M_d} \times 100 \quad (2)$$

where M_d is the weight of the samples before immersion in PBS medium and M_i is the weight of the samples after complete dehydration (%). All measurements were performed in triplicate ($n = 3$).

2.7 In vitro *drug release studies*

The release profile of MH from electrospun nanofiber mats was evaluated by measuring the UV–vis absorption of the drug in phosphate buffer solution (PBS, pH = 7.4) at the predetermined time intervals. The drug-loaded nanofiber mats were first cut into 2 × 2 cm pieces and then immersed into tubes containing 2 mL PBS solution individually. Tubes containing the samples were incubated in a thermal shaker at 37° C and 250 rpm. At specified time points, samples were taken out of the PBS solution and placed into a fresh buffer solution. The amount of drug released was determined from the absorbance at 233 nm by using a calibration curve based on simple aqueous standards**.** The experiments were performed in triplicate, and the mean values of the cumulative drug release percentage recorded were plotted as a function of time.

2.8 Drug release kinetics

To investigate the drug release mechanism, the MH release profiles from emulsion fibers were fitted to four popular mathematical equations such as zero order, first order, Higuchi and Korsmeyer-Peppas equations represented as Eqs. (3, 4, 5, 6).

$$Q = K_0 t \quad (3)$$

$$In(1 - Q) = -K_1 t \quad (4)$$

$$Q = K_h t^{1/2} \quad (5)$$

$$Q = K t^n \quad (6)$$

where Q is the fractional amount of drug release at time t; K_0, K_1, K_h, and K are the kinetic constants for zero order, first order, Higuchi, and Korsmeyer-Peppas model, respectively. n is the Korsmeyer-Peppas diffusion exponent, which is indicative of the drug release mechanism [47].

2.9 Cell culture

Cell proliferation on the developed electrospun mats was examined by culturing VHF93 human fibroblasts. Cell culture studies were carried out in 96 well-plate Petri dishes for 7 days with a cell seeding concentration of 5×10^3 cells/well in a growth medium consisting of DMEM + 10% FBS + 0.1 mg/mL penicillin/streptomycin, and the biocompatibility of the electrospun mats was studied on the 1st, 3rd, and 7th day. Initially, to ensure sterilization, the mats were placed in Petri dishes and exposed to ultraviolet (UV) radiation overnight. For optimization purposes, the electrospun mats were incubated in a growth medium for an hour at 37 °C in a humid 5% CO_2 incubator (SANYO). Then, the excess medium was discarded, and the electrospun mats were collected. This was followed by the initial culturing of the electrospun mats with the known amount of cells. Finally, the Petri dishes were kept in the incubator at 37 °C in humid 5% CO_2 for the 7 days of the culture period. To compare cell culture performance, a standard tissue culture polystyrene (TCPS) plate was used as a control.

To investigate cell viability and cytotoxicity at the given time point, a cytotoxicity detection kit (MTT from Glentham Life Sciences) was used. The absorbance values were measured at 560 nm wavelength (690 nm as Ref. Value) in an ELISA reader (PerkinElmer, Enspire). Each measurement was carried out in triplicate.

The cell attachment on/within the electrospun mats was investigated on the 3rd and 7th days of the culture using an inverted fluorescence microscope (Leica). For this, the growth medium was discarded on the specified days, and the electrospun mats were washed with PBS. After that, the fixation was performed with 4% formaldehyde for 30 min at room temperature, and then the mats were washed with PBS. For the staining, 1 µg/mL DAPI was added, and the samples were kept for 20 min at room temperature. Finally, the DAPI solution was discarded and the samples were placed between the slide and coverslip for the imaging.

The cellular morphology of VHF93 human fibroblasts on the electrospun mats was evaluated by SEM. The images were taken on the 7th day of cell cultivation. Therefore, the growth medium was discarded, and the samples with cells

were fixed with 4% glutaraldehyde. Next, the samples were dehydrated through the serial dilutions of ethanol and dried in the air. Before the analyses, the samples were sputter-coated with gold.

2.10 Statistical analysis

Statistical differences were determined using one-way analysis of variance (ANOVA) followed by Tuckey's test using IBM SPSS v24.0 Statistics software. The probability of the data was considered statistically significant for p values < 0.05, and statistically highly significant for p values < 0.01. The results were marked with (*) for $p < 0.05$, and (**) for $p < 0.01$.

3 Results and discussion

FTIR analysis was performed to characterize the chemical constitution of the nanofibers. Figure 2A demonstrates the FTIR spectra of electrospun MH, MH-HA, MH-KR, and MH-KR + HA fibers. The typical characteristic bands of PCL were observed in all composite fibers. The peaks at around 2941 cm^{-1} and 2864 cm^{-1} were attributed to asymmetric and symmetric $–CH_2$ stretching vibrations, respectively. Additionally, the intense and sharp peak at 1720 cm^{-1} was related to the carbonyl stretching vibration of the ester group. The peaks at around 1293 cm^{-1} and 1238 cm^{-1} were assigned to C-O and C–C stretching and asymmetric C–O–C stretching, respectively [48, 49]. According to the findings in our previous study on emulsion and coaxial nanofibers, the fact that the characteristic peaks of PEO, HA, and KR in the inner layer were not visible in FTIR spectra confirms that all nanofibers are successfully produced in the core/shell structure [45]. Similar results were presented by Liu et al. [50]. The pure MH shows typical characteristic peaks such as N–H asymmetric stretching (3370 cm^{-1}), N–H symmetric stretching (3296 cm^{-1} and 3152 cm^{-1}), C = N stretching (1661 cm^{-1}), and C-H asymmetric bending (1419.21 cm^{-1}) [51]. However, the characteristic peaks of MH were not observed in the spectra of all nanofibers. This indicates no solid chemical interaction between the drug and the polymer [23–52]. It is also evidence of effective encapsulation in core/shell nanofibers.

To demonstrate the crystalline structure and distribution of the drug in the nanofibers, XRD was studied. XRD patterns of pure HA, pure KR, pure MH powders, and composite nanofibers were given in Fig. 2B. The extracted pure HA powder (a) has an amorphous structure without a crystalline peak, which was reported by Jia et al. [53] and Hamad et al. [54]. The extracted pure KR powder (b) shows a broad diffraction peak at about 2θ value of 20.9° corresponded to the β-sheet structure [55, 56]. The sharp and intense peaks of pure MH (c) at 2θ values of 12.2°, 17.8°, and 24.5° indicate its highly crystalline nature, which is the agreement with the literature [57].

XRD pattern of MH fiber (d) illustrates two distinct diffraction peaks at 21.6° and 23.9° corresponding to the (110) and (200) planes of the crystal structure of PCL [58]. Similarly, the characteristic peaks of PCL were found in the patterns of all core/shell fibers, but the intensity of the peaks varied among the fibers. Compared to MH fiber (d), the intensity of the two sharp peaks in MH-KR (f) and MH-HA (e) fibers decreased. This can be related to the KR and HA inhibited crystallization of PCL. Also, MH-KR (f), MH-HA (e), and MH-KR-HA (g) fibers show a slight left shift for (110) lattice plane ~0.1°, ~0.2°, and ~0.4°, respectively. This might be assigned to the interaction between KR and HA with PCL. These findings were also in good agreement with the literature [59].

Moreover, MH-KR + HA fiber (g) exhibits much higher intense peaks than other fibers as the HA and KR content was less [60]. It can be seen that the crystalline peaks of MH (c) were not detected in the patterns of all core/shell fibers. This indicated that MH was highly distributed in the composite fibers [61], all the encapsulated drug was converted into an amorphous physical state and the original crystalline nature of the drug disappeared [50, 61].

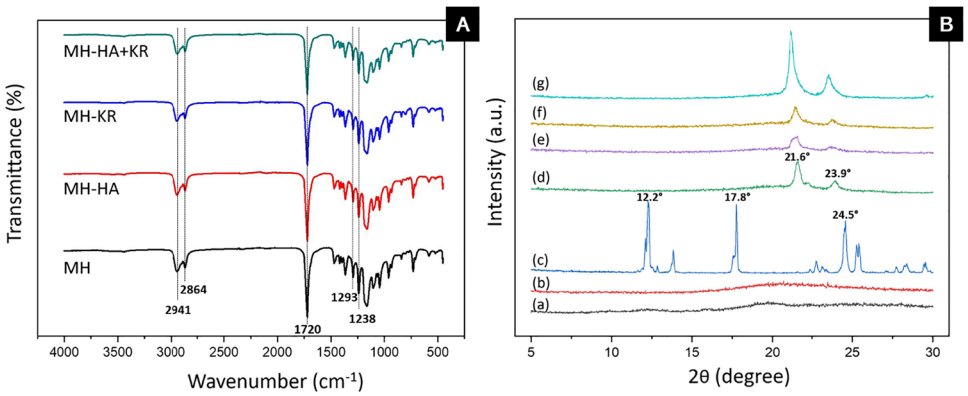

Fig. 2 **A** FTIR spectra of fiber samples, **B** XRD patterns of (a) pure HA, (b) pure KR, (c) pure MH, (d) MH, (e)MH-HA, (f) MH-KR, (g) MH-KR + HA fibers

The surface morphology and the average diameter of electrospun MH, MH-HA, MH-KR, and MH-HA + KR fibers were illustrated in Fig. 3. The SEM images show that all core/shell fibers have a smooth surface, bead-free structure, and relatively uniform diameters. No drug crystals were observed on the surface of the fibers. This demonstrates that the MH has successfully loaded into the fibers without any defects and that there was good drug-polymers-solvent compatibility [52–62]. As can be seen, the average diameter of the fibers decreased from 1.62 ± 63 µm to 0.54 ± 0.11 µm when the KR and HA were incorporated into the electrospun fibers. This phenomenon could be due to the fact that the conductivity of the emulsion solutions by the addition of KR and HA. Considering that KR is a polar biopolymer [34] and the polyanionic property of HA [63], mixing them separately and together into the solution will increase the conductivity of the solution. The higher conductivity of the solution can elongate the polymer jet easily and produce thinner and more uniform fibers [21–64].

The swelling capacity is a critical property of wound dressings because the excess exudate must be removed from the wound surface to control moisture balance [65]. It is known that the swelling capacity of electrospun mats varies according to the properties of the components. As shown in Fig. 4A, there is a marked increase in the maximum swelling capacity when HA and KR components are included in the fiber structure according to their hydrophilic nature. The absorption capability of MH-HA + KR (~ 800%) is at least twice that exhibited by the MH core–shell fiber mat (~ 350%). A similar result was previously described by a recent study which is about the hydrophilic plant (Centella Asiatica) that was included in the PCL-PVA nanofiber structure [66]. Figure 4B demonstrated the degradation of the fiber samples in PBS solution over 21 days. MH-HA + KR

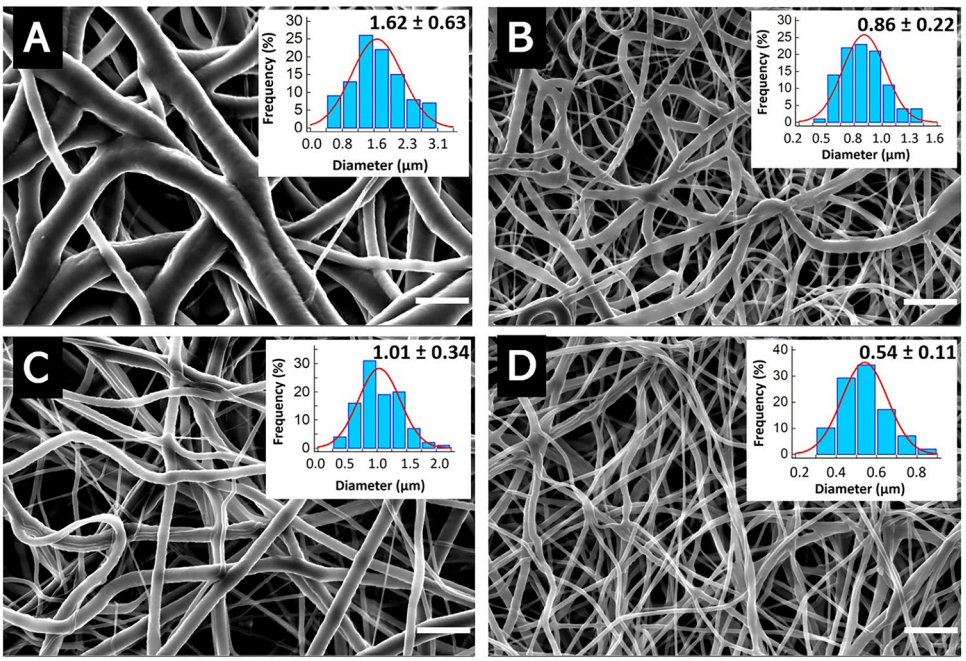

Fig. 3 SEM images and mean fiber diameter distributions of the fiber samples **A** MH, **B** MH-HA, **C** MH-KR, **D** MH-HA + KR (the scale bars in all images are 3 µm)

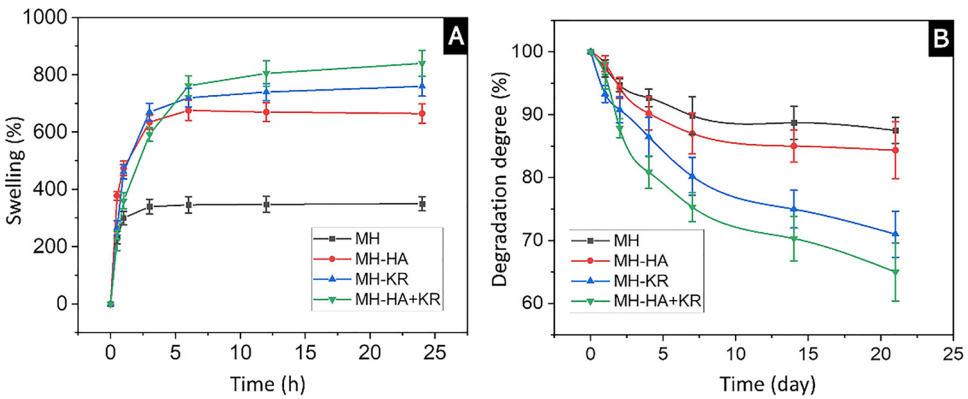

Fig. 4 Characterization of **A** swelling profile and **B** weight loss at pH = 7.4 of the produced fiber mats

had the highest weight loss versus other samples, as expected. MH-HA nanofibers degraded at a relatively slower rate in comparison to MH-KR. It can be attributed to the molecular weight of the produced HA (178.000 kDa) being much higher than that of keratin (~50 kDa), as reported in our previous study [45]. Furthermore, it has been shown that extensive chain entanglements occur between HA and PEO in a study in which high molecular weight HA is electrospun with PEO polymer [67]. The polymers can explain the difference in swelling and degradation rates between MH-HA and MH-KR in the core region of the M-HA sample are more tightly and effectively bonded to each other than in the other example.

The emulsion ES method, which enables fiber production in a core–shell structure, is a suitable technique for sustained drug release from drug-loaded fibers. Drug release studies were carried out by a UV spectrometer using a predetermined calibration curve at the absorbance of 233 nm. The drug release profiles for MH, MH-HA, MH-KR, and MH-HA + KR fiber mats are presented in Fig. 5A. All samples exhibited a two-stage release behaviour with an initial burst release followed by a sustained release. Furthermore, within the first 5 h, about 23.1 ± 4.4%, 32.4 ± 2.4%, 42.5 ± 3.23%, and 38.8 ± 5.1% of MH drug released from MH, MH-HA, MH-KR, and MH-HA + KR fiber mats, respectively (Fig. 5B). The possible reason for the higher burst release and total drug release amount in the samples, which include HA and KR, maybe due to the hydrophilic nature of HA and KR natural polymers as described swelling and degradation part. Besides, it was reported in a study that there was an inverse correlation between fiber diameter and drug release rate. The increased drug release in the presence of HA and KR can be attributed to the thinner fiber diameters of these samples [68].

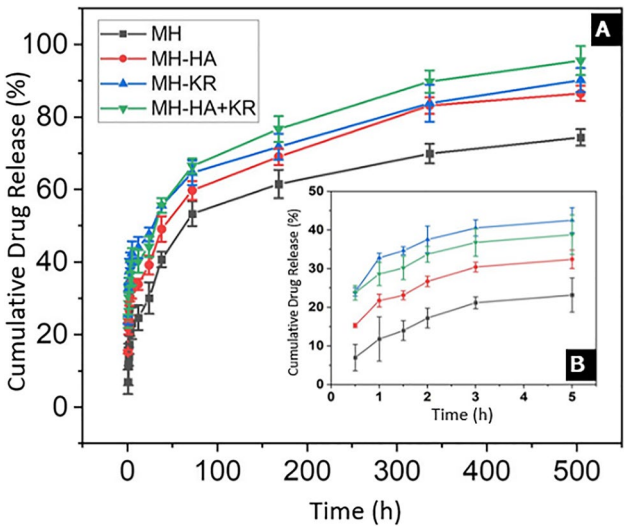

Fig. 5 **A** The cumulative MH release from MH, MH-HA, MH-KR, and MH-HA + KR samples during 21 days and **B** during the first 5 h

To understand drug release kinetics from fiber mats, release data were analyzed according to zero-order, first-order Higuchi, and Korsmeyer Peppas models and the kinetic parameters for each model (K_0, K_1, K_H, n) were listed in Table 2, as well as the regression coefficients (R^2).

For all samples, first order and Higuchi kinetics showed relatively good correlation coefficients, ranging from 0.85 to 0.95. The drug release mechanism was also analyzed according to the Korsmeyer Peppas model to have a deeper understanding of the release mechanism of MH drug from the emulsion fibers. In this model, the value of n describes the mechanism of drug release from a polymeric system. For a cylindrical system, $0.45 < n$ corresponds to a Fickian diffusion and $0.45 < n < 1$ refers the Non-Fickian diffusion [69]. The release of MH drug from all samples followed the Fickian diffusion mechanism, as indicated by n values ranging from 0.13 to 0.31. This means that drug release is mainly attributed to diffusion or penetration of the drug through the shell part (PCL) of the fibers, which is also frequently seen in the release of water-soluble drugs [70]. In a previous study, it was observed that formulations containing water-soluble drugs showed higher water uptake and erosion capacity than water-insoluble drugs. This was explained by the fact that the water-insoluble drug (as opposed to the water-soluble drug) was retarded in penetrating the solvent into the matrix, thus delaying swelling and corrosion [71].

The tetrazolium salt, MTT, an assay was carried out to determine the cytotoxicity and cell proliferation rate of the prepared fibrous mats [72]. MTT assay was performed with various time points of 1, 3, and 7 days. Results of the MTT assay are correlated with the cell proliferation and cell survival rate, which can be assessed with a spectrometer. As shown in Fig. 6A, no significant cell viability differences were observed for each group on the 1st and 3rd days,

Table 2 Kinetic models parameters of drug released from the electrospun fiber mats

Sample	Zero order		First order		Higuchi		Korsmeyer-Peppas	
	R^2	K_o	R^2	K_1	R^2	K_h	R^2	n
MH	0.7466	0.1266	0.8598	−0.0011	0.921	3.1046	0.9604	0.3134
MH-HA	0.7901	0.1338	0.9316	−0.0016	0.9453	3.2322	0.9562	0.1849
MH-KR	0.7992	0.1159	0.9555	−0.0017	0.9333	2.7818	0.9527	0.1324
MH-HA + KR	0.8117	0.1372	0.9524	−0.0024	0.9367	3.2896	0.9624	0.1540

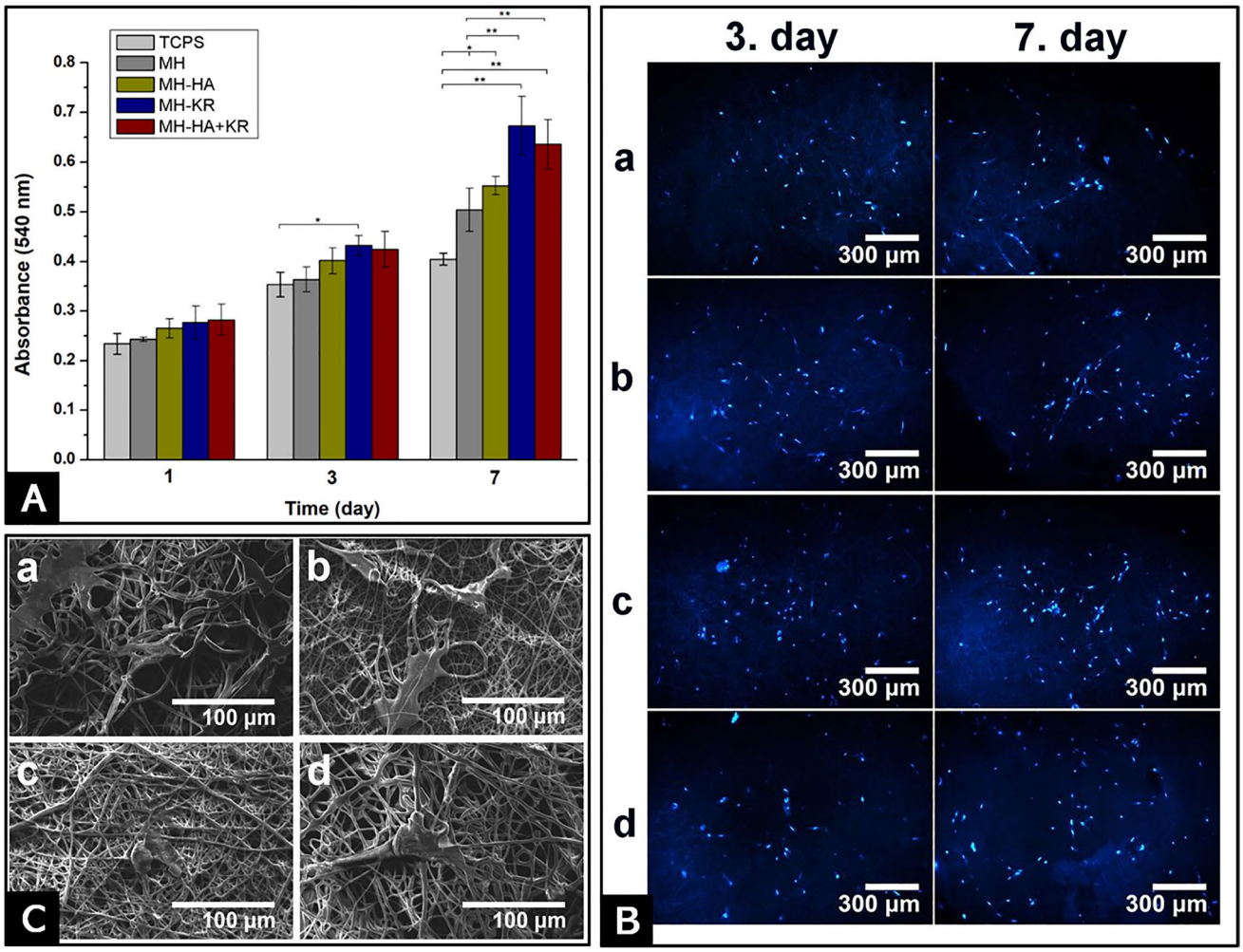

Fig. 6 **A** Absorbance values of the electrospun mats obtained by MTT assay at 540 nm (*$p<0.05$, **$p<0.01$; data presented are mean ± SD, $n=3$); **B** Fluorescence images of the electrospun mats at 3rd day (left) and 7th day (right) of cell growth for (a) MH (b) MH-HA; (c) MH-KR; (d) MH- HA + KR. Scale markers of 300 µm in all cases and **C** scanning electron microscopy (SEM) images of the cultured electrospun mats on the 7th day of cell growth: (a) MH; (b) MH-HA; (c) MH-KR; (d) MH-HA + KR. Scale markers of 100 µm in all cases

excluding the absorbance increase of MH-KR compared to the control group (TCPS) on the 3rd day of the study. Also, from this day, cell growth on the control revealed no absorbance increase, which indicates that cell cultivation on the TCPS plate passed to a stationary phase due to its 2-D morphology [72]. Contrary to the control, all the electrospun mats exhibited a notable steady increase in absorbance values, indicating no cytotoxicity to VHF93 fibroblasts. This increase can be explained by the 3-D structure of the electrospun mats, which provides cells with sufficient space to increase, particularly during the late stage of cell cultivation [73].

In terms of absorbance, the most notable differences were observed by the 7th day (Fig. 5), whereas the highest groups were MH-KR and MH-HA + KR. This result could be interpreted as the HA and KR compounds helping the fibroblast to proliferate and increase their life span. Also, the hydrophilic nature of HA and KR might be responsible for this absorbance value increase [74, 75]. Considering the electrospun mats containing HA, KR, and HA + KR compounds, it was observed that the highest absorbance is in the structure containing KR, followed by HA + KR and HA, respectively. As these similar results were discussed in our previous study [45], KR is widely reported as a compound that enhances cell viability [75, 76], For instance, Xing et al. [77] reported that keratin-PEO nanofibers at a weight ratio of 90:10 supported the proliferation of NIH 3T3 fibroblasts. Also, another study by Wu et al. demonstrated that cell proliferation was promoted when keratin was incorporated into a synthetic polymer, PCL [76]. On the other hand, the effect of HA on cellular response was reported previously to be dependent on the

dosage, inhibiting cell proliferation while promoting cell migration [78].

The obtained fluorescence images (Fig. 6B) verified sufficient support for cell attachment and proliferation on the previously dye stained electrospun mats. Additionally, according to the figure, while no significant cell density differences were observed, it can be seen that the characteristic fibroblast phenotype begins to occur at the end of the 7th of the cultivation.

The cell morphology and growth on the cultured electrospun mats were observed on the 7th day by SEM. As it can be seen in Fig. 6C, cells proliferated on all developed electrospun mats. One can observe that, particularly for the 7th day, the cells attached to the surface of the electrospun mats by their filopodia and exhibited flat morphology compared to the 3rd day.

4 Conclusion

Novel drug delivery systems based on core–shell fibers containing bioactive natural polymers (HA, KR) and a diabetic drug (MH) were successfully prepared by emulsion ES. SEM results showed that all samples had smooth and beadless structures while the HA and KR incorporation induced the formation of thinner fibers compared to neat core–shell fibers. The absence of characteristic bands of core polymers in the FTIR spectra supports the existence of core–shell structure. The swelling capacity of fibers containing KR and MH is at least twice that of neat core–shell fibers. It was observed that the degradation rates of the samples varied between 10 and 40% at the end of 21 days with the accelerating effect of hydrophilic HA and KR. The kinetic results indicated that MH release from all samples followed the first order and Higuchi model kinetics. When fitted to the Korsmeyer-Peppas, it was observed to follow a Fickian diffusion mechanism ($n < 0.45$). According to in vitro studies, all produced mats did not show any toxic effects on VHF93 fibroblasts. Furthermore, cell proliferation was higher in electrospun mats with HA and KR inclusion compared to pure mats and the control group. Also, fluorescence microscopy analyses and SEM revealed that the produced mats provided an appropriate environment for the fibroblast cells. MH- KR + HA can be considered the most suitable sample as a drug carrier thanks to its finer structure, high viability and favorable drug release behavior among others. Overall, this study strengthens the idea that HA and KR-based core–shell fibers can be a new scaffold as a drug carrier system for diabetic wound dressing.

Acknowledgements The authors wish to thank the Biomedical Imaging and Diagnostic Systems Development Laboratory at Marmara University, Istanbul.

Funding This research was funded by the BAPKO, Marmara University, grant number FEN-B-121218–0614″ and TUBITAK, Turkey, grant number 218S270.

Declarations

Competing interests The authors declare no competing interests.

References

1. S. Rahmani, D. Mooney, Diabet Foot, 247–256 (2018). https://doi.org/10.1007/978-3-319-89869-8_15
2. F.L. Bowling, S.T. Rashid, A.J.M. Boulton, Nat Rev Endocrinol **11**, 606–616 (2015). https://doi.org/10.1038/nrendo.2015.130
3. A. Wali, M. Gorain, S. Inamdar, G. Kundu, M. Badiger, A.C.S. Appl, Bio Mater **2**, 4324–4334 (2019). https://doi.org/10.1021/acsabm.9b00589
4. S. Ahmed, S. Ikram, Achiev. Life Sci **10**, 27–37 (2016). https://doi.org/10.1016/j.als.2016.04.001
5. L.I.F. Moura, A.M.A. Dias, E. Carvalho, H.C. De Sousa, Acta Biomater **9**, 7093–7114 (2013). https://doi.org/10.1016/j.actbio.2013.03.033
6. G. Han, R. Ceilley, Adv Ther **34**, 599–610 (2017). https://doi.org/10.1007/s12325-017-0478-y
7. A. Memic, T. Abudula, H.S. Mohammed, K. Joshi Navare, T. Colombani, S.A. Bencherif, ACS Appl. Bio Mater **2**, 952–969 (2019). https://doi.org/10.1021/acsabm.8b00637
8. M. Jannesari, J. Varshosaz, M. Morshed, M. Zamani, Int J Nanomedicine **6**, 993–1003 (2011). https://doi.org/10.2147/ijn.s17595
9. L.N. Kasiewicz, K.A. Whitehead, Biomater Sci **5**, 1962–1975 (2017). https://doi.org/10.1039/c7bm00264e
10. J.S. Boateng, K.H. Matthews, H.N.E. Stevens, G.M. Eccleston, J. Pharm Sci **97**, 2892–2923 (2008). https://doi.org/10.1002/jps.21210
11. Y.O. Kang, I.-S. Yoon, S.Y. Lee, D.-D. Kim, S.J. Lee, W.H. Park, S.M. Hudson, J Biomed Mater Res B Appl Biomater **92**, 568–576 (2010). https://doi.org/10.1002/jbm.b.31554
12. S. Peng, G. Jin, L. Li, K. Li, M. Srinivasan, S. Ramakrishna, J. Chen, Chem Soc Rev **45**, 1225–1241 (2016). https://doi.org/10.1039/c5cs00777a
13 D. Santos, D. Martins, I.S. Leite, A.L. de Bukzem, R.P. de Oliveira Santos, E. Frollini, N.M. Inada, S.P. Campana-Filho, Carbohydr Polym **186**, 110–121 (2018). https://doi.org/10.1016/j.carbpol.2018.01.045
14. V. Andreu, G. Mendoza, M. Arruebo, S. Irusta, Materials (Basel) **8**, 5154–5193 (2015). https://doi.org/10.3390/ma8085154
15. D.R. Figueira, S.P. Miguel, K.D. de Sá, I.J. Correia, Int J Biol Macromol **93**, 1100–1110 (2016). https://doi.org/10.1016/j.ijbiomac.2016.09.080
16. B.P. Antunes, A.F. Moreira, V.M. Gaspar, I.J. Correia, Carbohydr Polym **130**, 104–112 (2015). https://doi.org/10.1016/j.carbpol.2015.04.072
17 Y. Pilehvar-Soltanahmadi, M. Dadashpour, A. Mohajeri, A. Fattahi, R. Sheervalilou, N. Zarghami, Mini-Reviews Med Chem **18**, 414–427 (2018). https://doi.org/10.2174/1389557517666170308112147
18. G.M. Lanno, C. Ramos, L. Preem, M. Putrins, I. Laidmaë, T. Tenson, K. Kogermann, ACS Omega **5**, 30011–30022 (2020). https://doi.org/10.1021/acsomega.0c04402
19. L.E. Sperling, K.P. Reis, P. Pranke, J.H. Wendorff, Drug Discov. Today **21**, 1243–1256 (2016). https://doi.org/10.1016/j.drudis.2016.04.024

20. S. Liu, M. Qin, C. Hu, F. Wu, W. Cui, T. Jin, C. Fan, Biomaterials **34**, 4690–4701 (2013). https://doi.org/10.1016/j.biomaterials.2013.03.026
21. S. Yan, L. Xiaoqiang, L. Shuiping, M. Xiumei, S. Ramakrishna, Colloids Surfaces B Biointerfaces **73**, 376–381 (2009). https://doi.org/10.1016/j.colsurfb.2009.06.009
22. A.L. Yarin, Polym Adv Technol **22**, 310–317 (2011). https://doi.org/10.1002/pat.1781
23. N. Cai, C. Han, X. Luo, G. Chen, Q. Dai, & F. Yu, Macromol Mater Eng **302**, (2017). https://doi.org/10.1002/mame.201600364
24. N.E. Zander, Polymers (Basel) **5**, 19–44 (2013). https://doi.org/10.3390/polym5010019
25. Y. Yang, X. Li, W. Cui, S. Zhou, R. Tan, C. Wang, J Biomed Mater Res - Part A **86**, 374–385 (2008). https://doi.org/10.1002/jbm.a.31595
26. X. Xu, X. Zhuang, X. Chen, X. Wang, L. Yang, X. Jing, Macromol Rapid Commun **27**, 1637–1642 (2006). https://doi.org/10.1002/marc.200600384
27. H. Cheng, X. Yang, X. Che, M. Yang, G. Zhai, Mater Sci Eng C **90**, 750–763 (2018). https://doi.org/10.1016/j.msec.2018.05.007
28. R. Tylingo, G. Gorczyca, S. Mania, P. Szweda, S. Milewski, React Funct Polym **103**, 131–140 (2016). https://doi.org/10.1016/j.reactfunctpolym.2016.04.008
29. X. Liu, L.H. Nielsen, S.N. Kłodzińska, H.M. Nielsen, H. Qu, L.P. Christensen, J. Rantanen, M. Yang, Eur J Pharm Biopharm **123**, 42–49 (2018). https://doi.org/10.1016/j.ejpb.2017.11.004
30. R.L. Fischer, M.G. McCoy, S.A. Grant, J Mater Sci Mater Med **23**, 1645–1654 (2012). https://doi.org/10.1007/s10856-012-4641-3
31 P. Makvandi, G.W. Ali, F. Della Sala, W.I. Abdel-Fattah, A. Borzacchiello, Carbohydr Polym **223**, 115023 (2019). https://doi.org/10.1016/j.carbpol.2019.115023
32. Y. Hussein, E.M. El-Fakharany, E.A. Kamoun, S.A. Loutfy, R. Amin, T.H. Taha, S.A. Salim, M. Amer, Int J Biol Macromol **164**, 667–676 (2020). https://doi.org/10.1016/j.ijbiomac.2020.07.126
33. C.H. Yao, C.Y. Lee, C.H. Huang, Y.S. Chen, K.Y. Chen, Mater Sci Eng C **79**, 533–540 (2017). https://doi.org/10.1016/j.msec.2017.05.076
34. Y. Wang, P. Li, P. Xiang, J. Lu, J. Yuan, J. Shen, J Mater Chem B **4**, 635–648 (2016). https://doi.org/10.1039/c5tb02358k
35. M.I. Morasso, M. Tomic-Canic, Biol Cell **97**, 173–183 (2005). https://doi.org/10.1042/BC20040098
36. R.C. Marshall, D.F.G. Orwin, J.M. Gillespie, Electron Microsc Rev **4**, 47–83 (1991). https://doi.org/10.1016/0892-0354(91)90016-6
37. L. Bacakova, M. Zikmundova, J. Pajorova, A. Broz, E. Filova, A. Blanquer, R. Matejka, J. Stepanovska, P. Mikes, V. Jencova, E. Kuzelova Kostakova, & A. Sinica, Appl Nanobiotechnology, 1–30 (2020). https://doi.org/10.5772/intechopen.88744
38. L. Vileikyte, Diabetes Metab Res Rev **17**, 246–249 (2001). https://doi.org/10.1002/dmrr.216
39. S. Su, S.N. Korkmaz, U. Guven, S. Arslan, B. Karademir, M. SennarogluBostan, M.S. Eroglu, M. Uzun, C. Kalkandelen, M. Mahirogullari, M.T. Aurel, A. Ficai, D. Ficai, O. Gunduz, Med **55**, 1–13 (2019). https://doi.org/10.3390/medicina55100682
40. S.F. Spampinato, G.I. Caruso, R. De Pasquale, M.A. Sortino, S. Merlo, Pharmaceuticals **13**, 1–17 (2020). https://doi.org/10.3390/ph13040060
41. M.A. Carvalho-Filho, M. Ueno, S.M. Hirabara, A.B. Seabra, J.B.C. Carvalheira, M.G. de Oliveira, L.A. Velloso, R. Curi, M.J.A. Saad, Diabetes **54**, 959–967 (2005). https://doi.org/10.2337/diabetes.54.4.959
42. C.H. Lee, M.J. Hsieh, S.H. Chang, Y.H. Lin, S.J. Liu, T.Y. Lin, K.C. Hung, J.H.S. Pang, J.H. Juang, A.C.S. Appl, Mater Interfaces **6**, 3979–3986 (2014). https://doi.org/10.1021/am405329g
43 F.M. Barboza, W.M. Machado, L.R. Olchanheski Junior, J. de Paula, S.F. Zawadzki, D. Fernandes, P.V. Farago, Sci World J **2014**, 268107 (2014). https://doi.org/10.1155/2014/268107
44. M.A. Sanchez, A.P. Rodriguez, L.N. Monsalve, S. Georgiadou, Austin J Pharmacol Ther **8**, 1–8 (2020)
45. S. Su, T. Bedir, C. Kalkandelen, A.O. Bas, O. Gunduz, Eur Polym J J **142**, 110158 (2021). https://doi.org/10.1016/j.europolymj.2020.110158
46. F. Elshishiny, W. Mamdouh, ACS Omega **5**, 2133–2147 (2020). https://doi.org/10.1021/acsomega.9b02832
47. L. Li, J. Li, S. Si, L. Wang, C. Shi, Y. Sun, Z. Liang, S. Mao, Asian. J Pharm Sci **10**, 314–321 (2014). https://doi.org/10.1016/j.ajps.2014.09.002
48. M. Azizi, M. Azimzadeh, M. Afzali, M. Alafzadeh, S.H. Mirhosseini, J Adv Mater Process **6**, 34–46 (2018)
49. C. Mouro, M. Simões, I.C. Gouveia, Adv Polym Technol **2019**, 1–11 (2019). https://doi.org/10.1155/2019/9859506
50. M. Liu, X. Hao, Y. Wang, Z. Jiang, H. Zhang, J Mater Sci **55**, 16730–16743 (2020). https://doi.org/10.1007/s10853-020-05205-1
51. B.P. Panda, R. Krishnamoorthy, N.K.H. Shivashekaregowda, S. Patnaik, Nano. Biomed Eng **10**, 334–343 (2018). https://doi.org/10.5101/nbe.v10i4.p334-343
52. J. Hu, M.P. Prabhakaran, L. Tian, X. Ding, S. Ramakrishna, RSC Adv **5**, 100256–100267 (2015). https://doi.org/10.1039/c5ra18535a
53 Y. Jia, M. Huo, H. Huang, W. Fu, Y. Wang, J. Zhang, S. Jia, Proc Inst Mech Eng Part N J Nanoeng Nanosyst **229**, 41–48 (2015). https://doi.org/10.1177/1740349914529094
54. G.M. Hamad, T.H. Taha, E.E. Hafez, S. El Sohaimy, Am J Food Technol **12**, 72–85 (2017). https://doi.org/10.3923/ajft.2017.72.85
55. C. Mahajan, S. Tyagi, Int J Innov Res Adv Eng **6**, 2349–2163 (2019)
56. S. Li, X. H. Yang, Adv Mater Sci Eng **2014**, 1–7 (2014). https://doi.org/10.1155/2014/163678
57. S.C. Jagdale, S.A. Patil, B.S. Kuchekar, A.R. Chabukswar, J Young Pharm **3**, 197–204 (2011). https://doi.org/10.4103/0975-1483.83758
58. Y.F. Li, M. Rubert, H. Aslan, Y. Yu, K.A. Howard, M. Dong, F. Besenbacher, M. Chen, Nanoscale **6**, 3392–3402 (2014). https://doi.org/10.1039/c3nr06197c
59. L. Ma, X. Shi, X. Zhang, L. Li, Colloids Surfaces A Physicochem Eng Asp **583**, 123956 (2019). https://doi.org/10.1016/j.colsurfa.2019.123956
60. M. Eskitoros-Togay, Y.E. Bulbul, N. Dilsiz, J Appl Polym Sci **137**, 1–12 (2020). https://doi.org/10.1002/app.49273
61 J.M. Yang, L. ShengZha, D.G. Yu, J. Liu, Colloids Surfaces B Biointerfaces **102**, 737–743 (2013). https://doi.org/10.1016/j.colsurfb.2012.09.039
62. M.C.R. Simoes, S.M. Cragg, E. Barbu, F.B. De Sousa, J Mater Sci **54**, 5712–5725 (2019). https://doi.org/10.1007/s10853-018-03261-2
63. L. Li, Y. Qian, C. Jiang, Y. Lv, W. Liu, L. Zhong, K. Cai, S. Li, L. Yang, Biomaterials **33**, 3428–3445 (2012). https://doi.org/10.1016/j.biomaterials.2012.01.038
64. A.M. Moydeen, M.S. Ali Padusha, E.F. Aboelfetoh, S.S. Al-Deyab, M.H. El-Newehy, Int J Biol Macromol **116**, 1250–1259 (2018). https://doi.org/10.1016/j.ijbiomac.2018.05.130
65. G. Dabiri, E. Damstetter, T. Phillips, Adv Wound Care (2016). https://doi.org/10.1089/wound.2014.0586
66. C. Mouro, R. Fangueiro, I.C. Gouveia, Polymers (Basel) **12**, 1–18 (2020). https://doi.org/10.3390/polym12112653
67. H. Chen, X. Chen, H. Chen, X. Liu, J. Li, J. Luo, A. He, C.C. Han, Y. Liu, S. Xu, Membranes (Basel) **10**, 1–13 (2020). https://doi.org/10.3390/membranes10090217

68. Y. Wang, Z. Li, P. Shao, S. Hao, W. Wang, Q. Yang, B. Wang, Mater Sci Eng C **44**, 109–116 (2014). https://doi.org/10.1016/j.msec.2014.08.015
69. P.L. Ritger, N.A. Peppas, J Control Release (1987). https://doi.org/10.1016/0168-3659(87)90034-4
70. A. Radisavljevic, D.B. Stojanovic, S. Perisic, V. Djokic, V. Radojevic, M. Rajilic-Stojanovic, P.S. Uskokovic, Eur J Pharm Sci **124**, 26–36 (2018). https://doi.org/10.1016/j.ejps.2018.08.023
71. S. Chakraborty, M. Khandai, A. Sharma, C.N. Patra, V.J. Patro, K.K. Sen, Acta Pharm **59**, 313–323 (2009). https://doi.org/10.2478/v10007-009-0025-8
72 A.O. Basar, S. Castro, S. Torres-Giner, J.M. Lagaron, H. TurkogluSasmazel, Mater Sci Eng C **81**, 459–468 (2017). https://doi.org/10.1016/j.msec.2017.08.025
73. H.T. Sasmazel, M. Gumusderelioglu, A. Gurpinar, M.A. Onur, Biomed Mater Eng **18**, 119–128 (2008). https://doi.org/10.3233/BME-2008-0515
74. W.M. Payne, D. Svechkarev, A. Kyrychenko, A.M. Mohs, Carbohydr. Polym **182**, 132–141 (2018). https://doi.org/10.1016/j.carbpol.2017.10.054
75. A. Shavandi, T.H. Silva, A.A. Bekhit, A.E.-D.A. Bekhit, Biomater Sci **5**, 1699–1735 (2017). https://doi.org/10.1039/C7BM00411G
76. P. Wu, X. Dai, K. Chen, R. Li, Y. Xing, Int J Biol Macromol **114**, 1168–1173 (2018). https://doi.org/10.1016/j.ijbiomac.2018.03.157
77. Z.C. Xing, J. Yuan, W.P. Chae, I.K. Kang, S.Y. Kim, Int Conf Nanotechnol Biosensors **2**, 120–124 (2011)
78. D.G. Boeckel, R.S.A. Shinkai, M.L. Grossi, E.R. Teixeira, Oral Surg. Oral Med Oral Pathol Oral Radiol (2014). https://doi.org/10.1016/j.oooo.2012.07.486